the plant journal

SEB SOCIETY FOR EXPERIMENTAL BIOLOGY

The Plant Journal (2025) **122,** e70135 doi: 10.1111/tpj.70135

Role of an endodermis-specific *miR858b-MYB1L* module in the regulation of Taxol biosynthesis in *Taxus mairei*

Chunna Yu*, Danjin Zhang, Lingxiao Zhang, Zijin Fang, Yibo Zhang, Wanting Lin, Ruoyun Ma, Mengyin Zheng, Enhui Bai and Chenjia Shen*

College of Life and Environmental Sciences, Hangzhou Normal University, Hangzhou 311121, China

Received 10 November 2024; revised 27 February 2025; accepted 22 March 2025.
*For correspondence (e-mail shencj@hznu.edu.cn and yuchunna@hznu.edu.cn)

SUMMARY

Taxol, a chemotherapeutic agent widely used for treating various cancers, is extracted from the stems of *Taxus mairei*. However, current knowledge regarding the effects of stem tissue and age on Taxol accumulation is limited. We employed matrix-assisted laser desorption/ionization mass spectrometry to visualize taxoids in stem section sections of varying ages from *T. mairei*. Laser capture microdissection integrated with data-dependent acquisition–MS/MS analysis identified that several Taxol biosynthesis pathway-related enzymes were predominantly produced in the endodermis, elucidating the molecular mechanisms underlying endodermis-specific Taxol accumulation. We identified an endodermis-specific MYB1-like (MYB1L) protein and proposed a potential function for the *miR858-MYB1L* module in regulating secondary metabolic pathways. DNA affinity purification sequencing analysis produced 92 506 target peaks for MYB1L. Motif enrichment analysis identified several *de novo* motifs, providing new insights into MYB recognition sites. Four target peaks of MYB1L were identified within the promoter sequences of Taxol synthesis genes, including *TBT*, *DBTNBT*, *T13OH*, and *BAPT*, and were confirmed using electrophoretic mobility shift assays. Dual-luciferase assays showed that MYB1L significantly activated the expression of *TBT* and *BAPT*. Our data indicate that the *miR858b-MYB1L* module plays a crucial role in the transcriptional regulation of Taxol biosynthesis by up-regulating the expression of *TBT* and *BAPT* genes in the endodermis.

Keywords: MiR858, Taxol, axol biosynthesis, MYB, DAP-seq.

INTRODUCTION

Taxol (also known as paclitaxel) is isolated from the stem bark of *Taxus brevifolia* and has been approved as a potent anti-cancer drug for the treatment of various cancers (Gallego-Jara et al., 2020). However, the limited availability of naturally occurring Taxol, due to its low natural abundance in Taxus bark, has led to increased costs (Wani & Horwitz, 2014) and has contributed to the decline of *Taxus* populations as a result of large-scale extraction (Chybicki & Oleksa, 2018). Therefore, understanding the regulatory mechanisms that control the abundance of Taxol in natural *Taxus* tissues is essential for improving yield and reducing the costs associated with this drug.

The Taxol biosynthetic pathway comprises approximately 20 steps that start with the diterpenoid precursor, geranylgeranyl pyrophosphate (GGPP) (Jennewein et al., 2004). GGPP is cyclized to synthesize taxadiene, which serves as the core diterpene skeleton of Taxol, by the enzyme taxadiene synthase (TS) (Wildung & Croteau, 1996). Subsequently, the taxadiene skeleton undergoes hydroxylation and acylation to form baccatin III (BAC) through a series of taxoid hydroxylases and 10-deacetylbaccatin III-10-*O*-acetyl-transferase (DBAT) (Zhou et al., 2019). A C13-side chain is assembled and ligated to BAC to produce baccatin III 13-*O*-(3-amino, 3-phenylpropanoyl) transferase (BAPT). Finally, the enzyme 3′-*N*-debenzoyl-2′-deoxytaxol *N*-benzoyl transferase (DBTNBT) plays an important role in the synthesis of Taxol from 3′-*N*-debenzoyl-2′-deoxytaxol (Kaspera & Croteau, 2006; Zhang et al., 2024). Recently, taxane oxetanase 1 (TOT1) has been identified as a novel bifunctional cytochrome P450 enzyme involved in the formation of the Taxol oxetane (Jiang et al., 2024).

The distribution of active ingredients in medicinal plants is often uneven (Zhan, Liang, et al., 2024; Zhan, Zang, et al., 2024). Although Taxol was initially isolated from the bark of *T. brevifolia*, various taxoids have been detected in different stem tissues (Vance et al., 1994). Subsequent research has shown that taxoids are distributed unevenly across stem tissues. For example, baccatin IV, taxine B, and taxinine M, located in the cortex, and

taxuspine W, located in the vascular tissue, were simultaneously detected in the stem tissue of *T. baccata* (Arendowski & Ruman, 2017). In addition, tissue age has also been shown to significantly affect the biosynthesis of taxoids in *Taxus* trees (Demidova et al., 2023). Taxol and 10-deacetyl baccatin III (10-DAB III) levels were found to be significantly higher in 5-year-old *T. media* trees than in three-year-old trees (Shi et al., 2010). Recent technological advancements have allowed researchers to visualize the distribution of active compounds in various plant tissues (Li et al., 2023).

Many transcription factors (TFs) are reportedly involved in the hormone-related regulation of Taxol biosynthesis (Kuang et al., 2019; Yu et al., 2023). For example, a basic helix-loop-helix TF, MYC2a, controls the jasmonic acid (JA)-mediated Taxol biosynthetic pathway by recognizing the T/G-box, G-box, and E-box in the promoter region of Taxol biosynthesis-related genes (Zhang et al., 2018). WRKY33 positively regulates the salicylic acid (SA)-mediated Taxol biosynthetic pathway by up-regulating the expression of the *TS* and *DBAT* genes (Chen et al., 2021). MYB29a is involved in abscisic acid (ABA)-related Taxol biosynthesis by up-regulating the expression of the *TS*, taxane 5α-hydroxylase (*T5OH*), and *DBTNBT* genes (Cao et al., 2022). Previous studies have identified several Taxol biosynthesis-related MYB family members, including phloem-specific MYB3, female tree-specific MYB39, and stem endodermal cell-specific MYB47 (Yu et al., 2020; Yu et al., 2022; Yu et al., 2023). The identification of effective TFs may prove to be beneficial for improving the genetic makeup of *Taxus* species.

MicroRNAs (miRNAs) function as upstream regulators of various TFs. In plants, miRNAs are essential regulators involved in a range of biological processes, including secondary metabolism (Hobert, 2008). In *Taxus*, miRNA targets have been identified through degradome analysis (Fei et al., 2019). Interestingly, taxane 13β-hydroxylase (T13OH) and taxane 2α-*O*-benzoyltransferase (TBT) were identified as direct targets of miR164 and miR171, respectively, in the first report describing the potential roles of miRNAs in Taxol biosynthesis (Hao et al., 2012). In *T. media* callus cells, miRNAs play essential roles in the regulation of secondary metabolite biosynthesis by targeting several TF genes, including *ERF*, *WRKY*, and *SPL* (Chen, Zhang, et al., 2020). Recently, miR5298b was shown to enhance Taxol accumulation by activating the NPR3-TGA6 complex, which directly binds to the TAACG motif within the promoter regions of *TS*, *T5OH*, and *T10OH* (Ying et al., 2023). The screening and identification of upstream regulators of Taxol biosynthesis-related TFs will further the understanding of the Taxol biosynthetic pathway.

Understanding how TFs regulate various biological processes in plants requires the identification and screening of specific *cis*-regulatory elements (CREs) in the promoters of downstream targets (Bobadilla & Tranel, 2024). CREs are composed of various DNA motifs, typically ranging from 6 to 30 base pairs in length, that function as specific binding sites for TFs (Schmitz et al., 2022). DNA affinity purification sequencing (DAP-seq) is a novel method for screening DNA-binding proteins and identifying the transcription regulatory network of specific TFs (O'Malley et al., 2016). This DAP-seq technology allows for the identification of novel targets of Taxol biosynthesis-related TFs. However, visual investigations of taxoid distribution across stem tissues of trees of varying ages remain relatively scarce.

In wild *Taxus* trees, the highest yield of Taxol was obtained from the stem bark (specifically, epidermal cells) (Das et al., 2023). In industrial production, branches of *Taxus* are harvested every year to be used as raw materials for Taxol extraction. Which age of stems is suitable as raw material for Taxol extraction is largely unknown. In our study, 1-year-old and 2-year-old stems were selected for DDA-MS/MS analysis. From an anatomical standpoint, Taxol primarily accumulates in epidermal cells (Yu et al., 2023). Here, we identified an endodermis-specific MYB1-like (MYB1L) protein and screened its potential downstream targets using DAP-seq analysis. Our findings further the understanding of the miRNA-TF regulatory pathway underlying Taxol biosynthesis and offer a potential explanation for the tissue-specific accumulation of Taxol.

RESULTS

Analysis of MS imaging data

1-year-old (O) and 2-year-old (T) stems of *T. mairei* were harvested for MS imaging analysis (Figure 1a). Matrix-Assisted Laser Desorption Ionization Mass Spectrometry Imaging (MALDI-MSI) was performed to examine the tissue-specific accumulation of taxoids (Figure S1a). The average mass spectrogram from the MS analysis is shown in Figure 1b. Taxoid accumulation patterns in the stems were examined by segmentation analysis, which generated various colored maps with an average of 29 866 site points (Figure S1b,c). K means-based maps revealed the presence of several tissue-specific metabolite accumulation patterns in the samples (Figure S1d). In total, 8026 MS features were obtained, 1760 of which were identified using the Bruker Library MS-Metabobase (Table S1).

PCA separated all identified MS features into five principal components (PCs) associated with various known stem tissues: pith (PC1), xylem (PC2), phloem-endodermis (PC3), epidermis (PC4), and multi-tissues (PC5) (Figure 1c). The PC loading data for each MS feature is shown in Figure 1d. The number of tissue-specific MS features was quantified. Interestingly, metabolites exhibited a tendency to accumulate in the PC2 (1965 MS features) of O stems and PC3 (1454 MS features) of T stems (Figure 1e).

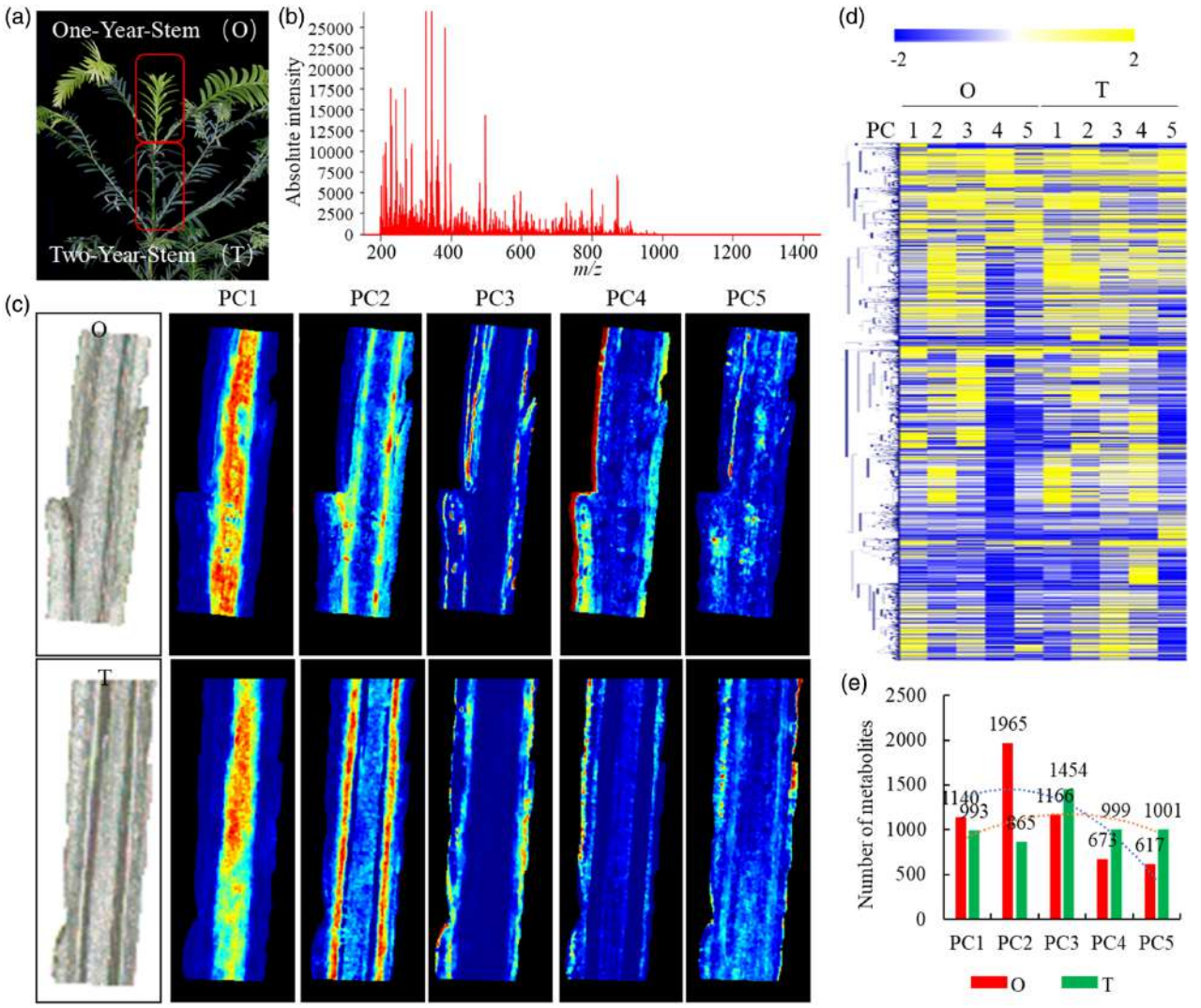

Figure 1. MS imaging analysis of the 1-year-old (O) and 2-year-old (T) *Taxus mairei* stems.
(a) A picture of O and T stems.
(b) The average mass spectrogram of MS imaging data.
(c) PCA of all the detected MS features from O and T stems. Five principal components (PCs) indicate different accumulation patterns of detected features in stems.
(d) Heatmap showing the relative accumulation levels of each detected features in five principal components (PCs). The heatmap scale ranges from −2 to +2 on a $\log_2$ scale.
(e) The number of tissue specifically accumulated MS features in O and T stems.

Visualization of taxoids in *T. mairei* stems

A total of seven different taxoids were identified by the MALDI-MSI analysis, including Taxol, three intermediates involved in Taxol biosynthesis, and three Taxol analogues (Figure 2a). Similar patterns of taxa-4(20),11(12)-dien-5α-yl acetate, a downstream product of TAT, were observed in both O and T stems. High concentrations of 10-DAB III, BAC, and Taxol were observed in O stems. Specifically, significant accumulation of 10-DAB III and BAC was found in the PC1 of O stems, while significant accumulation of Taxol occurred in the PC3 (Figure 2b,c). Regarding Taxol analogues, substantial accumulation of 10-deacetyl-7-xylosyl paclitaxel and 10-deacetyl Taxol C was observed in the PC3, whereas cephalomannine accumulated in the PC1 and PC2 (Figure 2d,e). It is worth mentioning that taxoid accumulation levels were generally higher in young stems compared to old stems for most taxoids.

Analysis of LCM integrated with DDA-MS/MS data

Cell types have distinct proteomes that are often underrepresented and intermixed in whole stem samples comprising multiple cell types. Manual separation of stem tissues can be

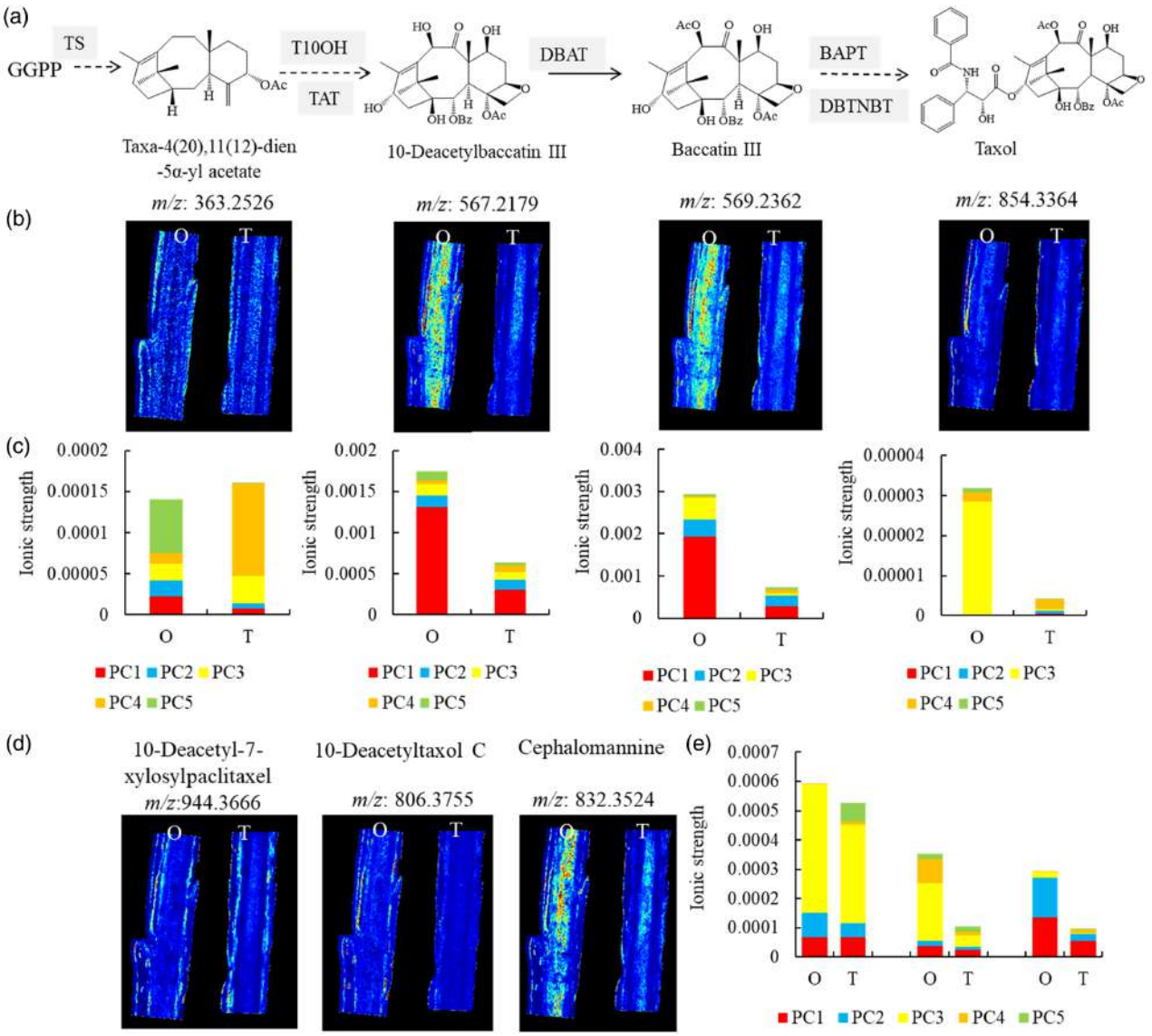

Figure 2. Visualization of taxoid accumulation in *Taxus mairei* stems.
(a) Overview of the Taxol biosynthesis pathway, including enzymes and metabolites.
(b) The accumulation level of taxa-4(20),11(12)-dien-5α-yl acetate, 10-deacetylbaccatin III, baccatin III, and Taxol was determined by the MALDI-IMS analysis. The color scale ranges from 0% to 100%. Blue indicated low accumulation and red indicated high accumulation.
(c) The proportion of Taxol and various taxoids in different stem tissues was shown by histogram.
(d) The accumulation of three Taxol analogues was determined by MALDI-IMS analysis. The color scale ranges from 0% to 100%. Blue indicated low accumulation and red indicated high accumulation.
(e) The proportion of Taxol analogues in different stem tissues was shown by histogram.

imprecise (Yu et al., 2020). Here, we performed data-dependent acquisition-Tandem Mass Spectrometry (DDA-MS/MS) analysis to examine the genetic mechanisms underlying the tissue-specific accumulation of taxoids in different aged stems. LCM was used to collect five distinct tissues from each stem sample, labeled from 1 to 5 (Figure 3a–c). The precise location of each sampling point in both O and T stems is shown in Figure 3d. Analysis of two quality control parameters, protein FDR and protein abundance, indicated the reliability of all samples, with the exception of T-1 (Figure S2a,b). A total of 15 046 peptides, corresponding to 3145 protein groups, were identified across the various stem samples. Detailed information regarding the identified proteins is shown in Table S2. PCA separated all samples into different groups (Figure S2c), and the quantitative heatmap of total proteins is shown in Figure 3e.

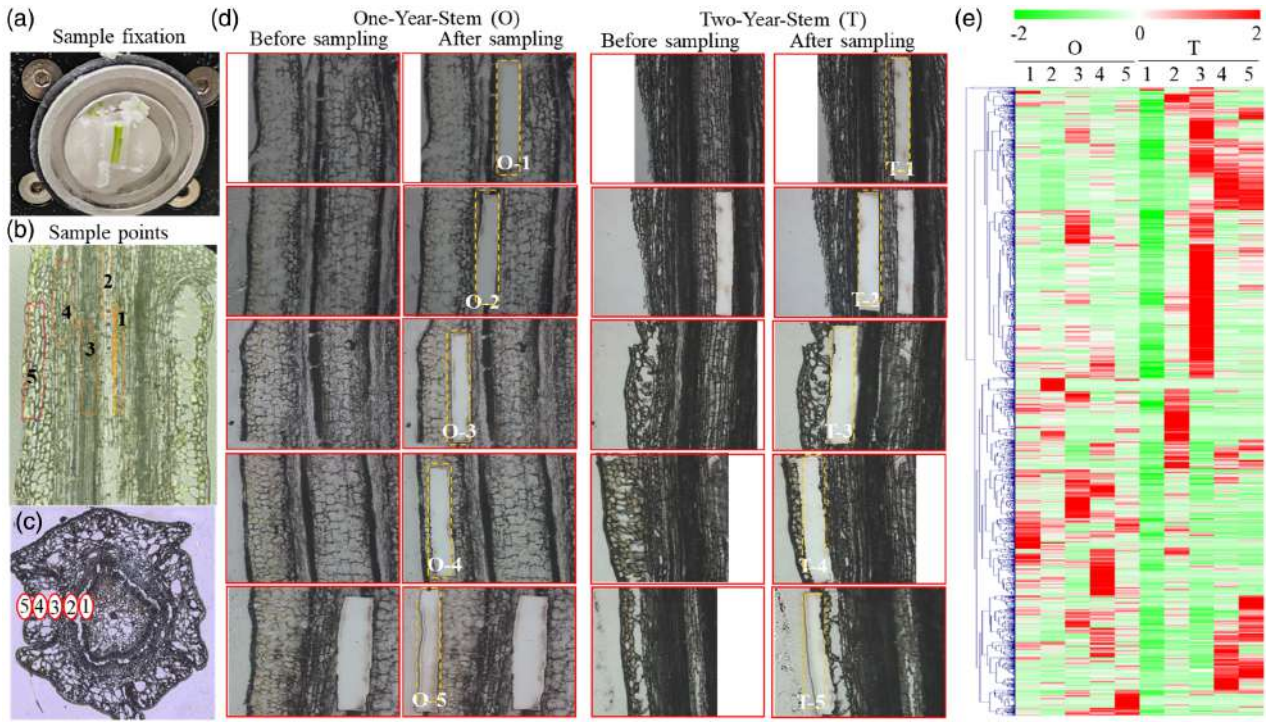

Figure 3. The basic information of LCM integrated with DDA-MS/MS analysis.
(a) A picture shows sample fixation and frozen sectioning.
(b) The position information of each sampling point (vertical cutting).
(c) The position information of each sampling point (cross cutting).
(d) The accurate location of each sampling point in both O and T stems.
(e) A heatmap of the abundance of proteins in the five sampling points from both O and T stems ($n = 3$). The heatmap scale ranges from −2 to +2 on a $\log_2$ scale.

Identification of differentially expressed proteins (DEPs) in different stem samples

The PC1 of the T stems was found to be hollow, and thus, only 24 proteins were identified in T-1. With the exception of T-1, the number of identified proteins in each sample varied from 1788 (T3) to 2819 (O5) (Figure 4a). Excluding unidentified proteins, several DEPs were detected across various comparisons (Figure 4b). Interestingly, most of the highly expressed DEPs in T stems were found to accumulate in the same locations as those in O stems.

Kyoto Encyclopedia of Genes and Genomes (KEGG) enrichment analysis categorized the DEPs into various metabolism-related pathways. In O stems, DEPs were found to be significantly enriched in several fundamental metabolic pathways, including starch and sucrose metabolism (O2/O3 and O4/O5) and lipoic acid metabolism (O4/O5). In T stems, significant enrichment of DEPs was observed in various secondary metabolic pathways, including monoterpenoid biosynthesis (T4/T5), degradation of flavonoids (T2/T3, T3/T4, and T4/T5), pyrimidine metabolism (T2/T3), ascorbate and aldarate metabolism (T3/T4), and glutathione metabolism (T4/T5). The DEPs were found to be significantly enriched in monoterpenoid biosynthesis (T2/O2, T4/O4, and T5/O5) (Figure 4c).

DDA-MS/MS analysis of the Taxol biosynthetic pathway

The methyl-D-erythritol phosphate (MEP) pathway provides an important precursor, GGPP, for diterpenoid biosynthesis (Yu et al., 2023). In this study, we detected 10 MEP pathway-related proteins, most of which were highly expressed in the O-3/T-3, O-3/T-4, and O-3/T-5 sample groups. Several members of the CYP725A subfamily have been shown to possess specific hydroxylase activities that are involved in the Taxol biosynthetic pathway (Xiong et al., 2021). In total, 16 CYP family members were detected; four CYP725A subfamily members were significantly expressed in the O-4 sample group (Figure 4d). Furthermore, eight Taxol biosynthesis-related enzymes, including T5OH1/2, TAT1/2, T2OH, T13OH, T10OH, and BAPT, were detected. Interestingly, all eight Taxol biosynthesis-related enzymes were significantly expressed in the O-4 sample group (Figure 4e).

Identification of PC3-specific *MYB1L* expression

Due to the relatively low throughput of LCM-DDA-MS/MS analysis, no suitable TFs were detected. In our previous

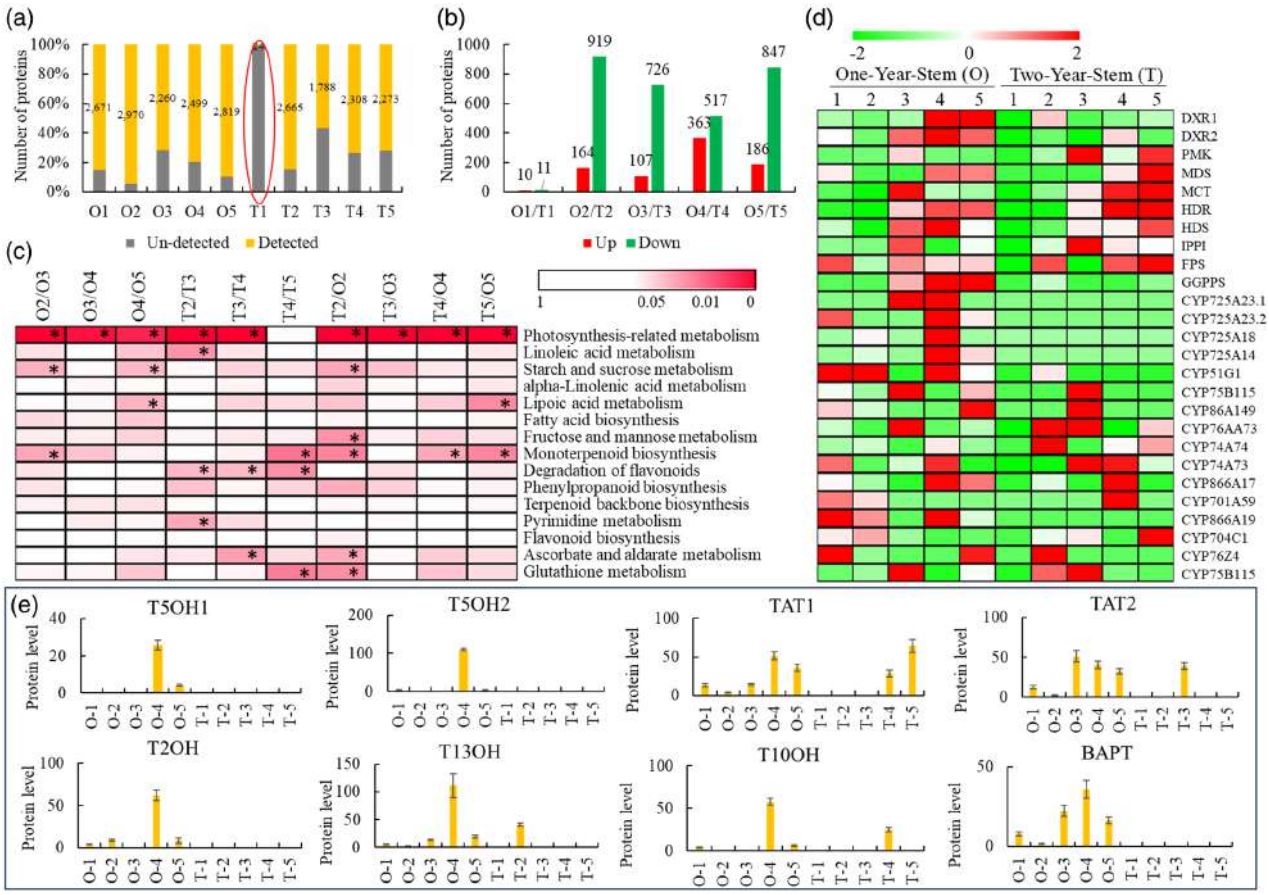

Figure 4. Identification of differentially produced proteins in different stem samples.
(a) The number of identified proteins in each sample group.
(b) The number of differentially produced proteins in various comparisons.
(c) Kyoto Encyclopedia of Genes and Genomes (KEGG) enrichment analysis of the differentially produced proteins into various metabolism-related categories. *Indicated significant changes at $P < 0.05$.
(d) DDA-MS/MS analysis of the MEP pathway-related proteins and CYP family members. The heatmap scale ranges from −2 to +2 on a $\log_2$ scale.
(e) DDA-MS/MS analysis of the Taxol biosynthesis pathway-related proteins.

study, we created a single-cell transcriptome atlas of the *T. mairei* stem (Yu et al., 2023). Utilizing the single-cell transcriptomic dataset, 18 tissue-specific expressed MYB family genes were identified (Figure 5a). Among the detected MYB family genes, the expression of *MYB35*, *MYB46*, *MYB18*, *PHL2*, *MYB21.1*, *MYB21.2*, *MYB6*, *MYB1L*, and *MYB57* displayed excellent cell coverage (>100 cells, Figure 5b). Cell-specific expression analyses showed that *MYB1L* (ctg5083_gene.1) was specifically expressed in Cluster 12, which corresponds to PC3 tissue, indicating that *MYB1L* is a PC3-specifically expressed gene (Figure 5c). *In situ* hybridization experiments confirmed that the positive signals of *MYB1L* were greatly enriched in the endodermis (Figure 5d). Compared to the T stems, the signals of *MYB1L* were highly detected in the O stems, indicating that MYB1L was significantly expressed in the young twigs of *T. mairei*. Multiple sequence alignment revealed that MYB1L possessed a complete R2R3 domain at the *N*-terminus, indicating that it is a typical R2R3-MYB subfamily member (Figure S3).

Prediction and validation of miRNA858b-MYB1L interactions

MYB family TFs are regulators of secondary metabolism in plants (Cao et al., 2020). In our study, we aimed to identify the upstream regulators of *MYB1L* by establishing and sequencing three independent libraries of sRNAs from *T. mairei* stems. The psRNA Target Server was utilized to predict potential targets of miRNAs, and a total of 2351 genes were predicted as targets of 483 miRNAs. Functional annotation revealed that each miRNA possessed several putative targets associated with various biological processes (Table S3). Gene Ontology (GO) enrichment analysis grouped all of the predicted targets into four categories, including transcriptional regulation, environmental response, secondary metabolism, and growth and

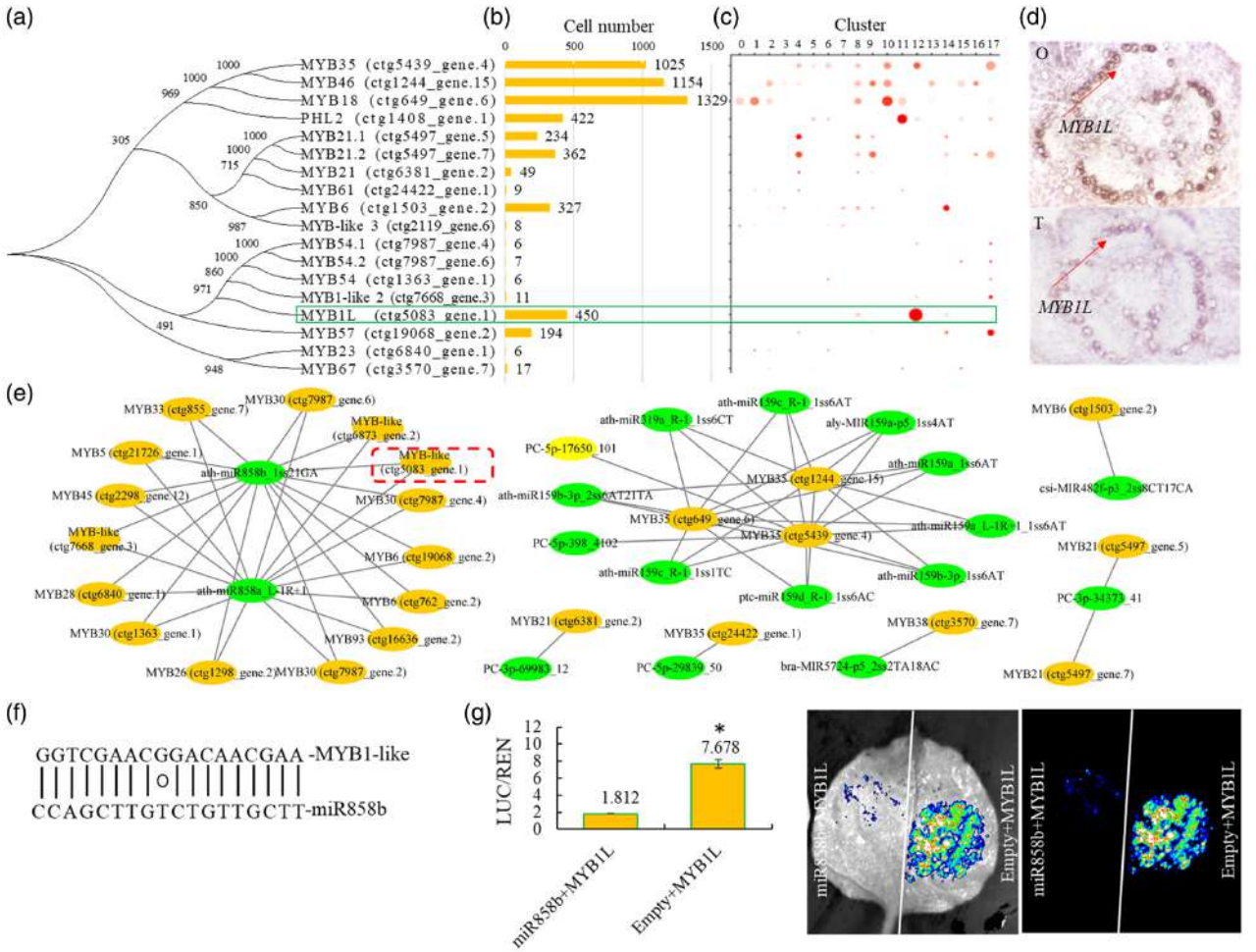

Figure 5. Identification of endodermis specifically expressed *MYB1L* and its upstream regulator miR858b.
(a) Phylogenetic tree of MYB family member with full-length sequences.
(b) The cell coverage of Taxol biosynthesis-related genes.
(c) Cell-specific expression analysis of MYB genes. Cluster 12 refers to endodermal cells.
(d) *In situ* hybridizations of *T. mairei* stems with MYB1L probe to illustrate its tissue-specific expression pattern.
(e) Prediction of a miRNA-MYB regulatory network in *T. mairei*. Red box indicated *MYB1L*.
(f) Base pairing of *MYB1L* and *miRNA858b*.
(g) The regulatory role of miR858b in the expression of the *MYB1L* gene was determined using a dual-luciferase transient expression system. *Indicated significant changes at $P < 0.05$.

development (Figure S4a). KEGG enrichment analysis suggested that the predicted targets may be involved in multiple metabolic pathways (Figure S4b). Many miRNA target genes were associated with transcriptional regulation, highlighting the presence of numerous miRNA-TF regulatory modules in the stems of *T. mairei*.

In our study, we predicted a miRNA-MYB regulatory network in *T. mairei*. Two miRNA858 family (ath-miR858b_1ss21GA and ath-miRNA858a_L-1R + 1) were found to regulate 15 MYB family TF genes. In addition, three MYB35 encoding genes (ctg649_gene.6, ctg1244_gene.15, and ctg5439_gene.4) were found to be regulated by 11 miRNAs (Figure 5e). Specifically, *MYB1L* (ctg5083_gene.1) was identified as a target of miR858b (Figure 5f). Subsequently, we employed a transient Dual-LUC reporter assay to determine the regulatory role of miR858b in *MYB1-like* gene expression. The LUC/REN ratio of the sample expressing *MYB1L* was 7.678, while co-expression of miR858b and *MYB1L* reduced the LUC/REN value to 1.812, confirming the interaction between miR858b and *MYB1L* (Figure 5g).

Identification of MYB1L-binding regions by DAP-seq

Although several studies have examined the biological roles of MYB family members from *Taxus*, their targets have not been fully identified. Here, we aimed to identify genome-wide binding sites for MYB1L and its potential target genes. The expression of MYB1L protein was validated using Western blotting analysis, which showed that

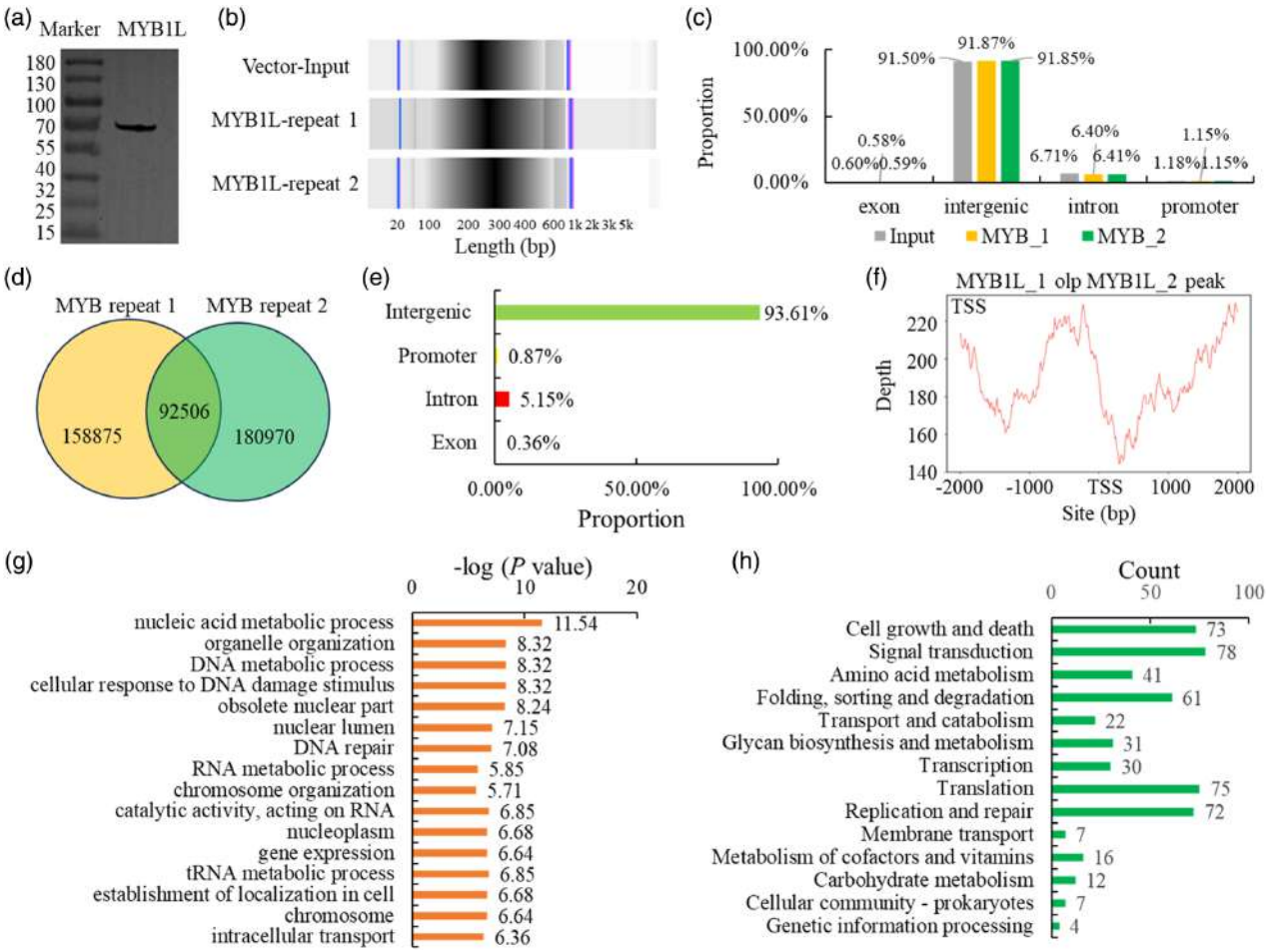

Figure 6. Identification of MYB1L-binding regions by DAP-seq.
(a) Using antibody for western blot detection of expressed MYB1L protein.
(b) Establishment of three libraries and quality inspection for enriched products.
(c) Genome-wide location analysis of the MYB1L target peaks.
(d) Venn analysis of overlap target peaks from MYB1L-repeat1 and MYB1L-repeat2 libraries.
(e) Genome-wide location analysis of the target peaks between MYB1L-repeat1 and MYB1L-repeat2 libraries.
(f) The overlap peak frequencies near the transcription start site.
(g) Gene Ontology (GO) enrichment analysis of the target genes of MYB1L.
(h) Kyoto Encyclopedia of Genes and Genomes (KEGG) enrichment analysis of the target genes of MYB1L.

MYB1L has a molecular weight of 65 kDa (Figure 6a). Next, we constructed three libraries of input and two MYB1L repeats. Quality inspection of the test libraries demonstrated that they were of high quality (Figure 6b). Using the Illumina platform, approximately 140 million raw reads were generated by DAP-seq (Table S4).

A substantial number of MYB1L target peaks were identified (Table S5). Genome-wide analysis revealed that the majority of the MYB1L target peaks were situated in the intergenic regions, with an average of 6.1% of target peaks located in the intron regions and an average of 1.16% found in the promoter regions (Figure 6c). Venn analysis revealed 92 506 overlapping target peaks (Figure 6d), of which 5.15% and 0.87% were located in intron and promoter regions, respectively (Figure 6e,f).

Analysis of potential MYB1L targets and binding motifs

To gain insight into the biological functions of MYB1L target genes, we next carried out GO and KEGG analyses. GO enrichment analysis revealed that the target genes of MYB1L were enriched in "nucleic acid metabolic process," "organelle organization," and "DNA metabolic process" (Figure 6g), while KEGG enrichment analysis identified "signal transduction" (78 genes), "translation" (75 genes), and "cell growth and death" (73 genes) genes (Figure 6h).

Analysis of the motifs in the peak regions allows further prediction of potential downstream target genes of MYB family members. Motif enrichment analysis showed that the top five known MYB1L binding motifs were "AGGGTTTAGGGTTTA" (P = 1e-3995), "TAAACCCT"

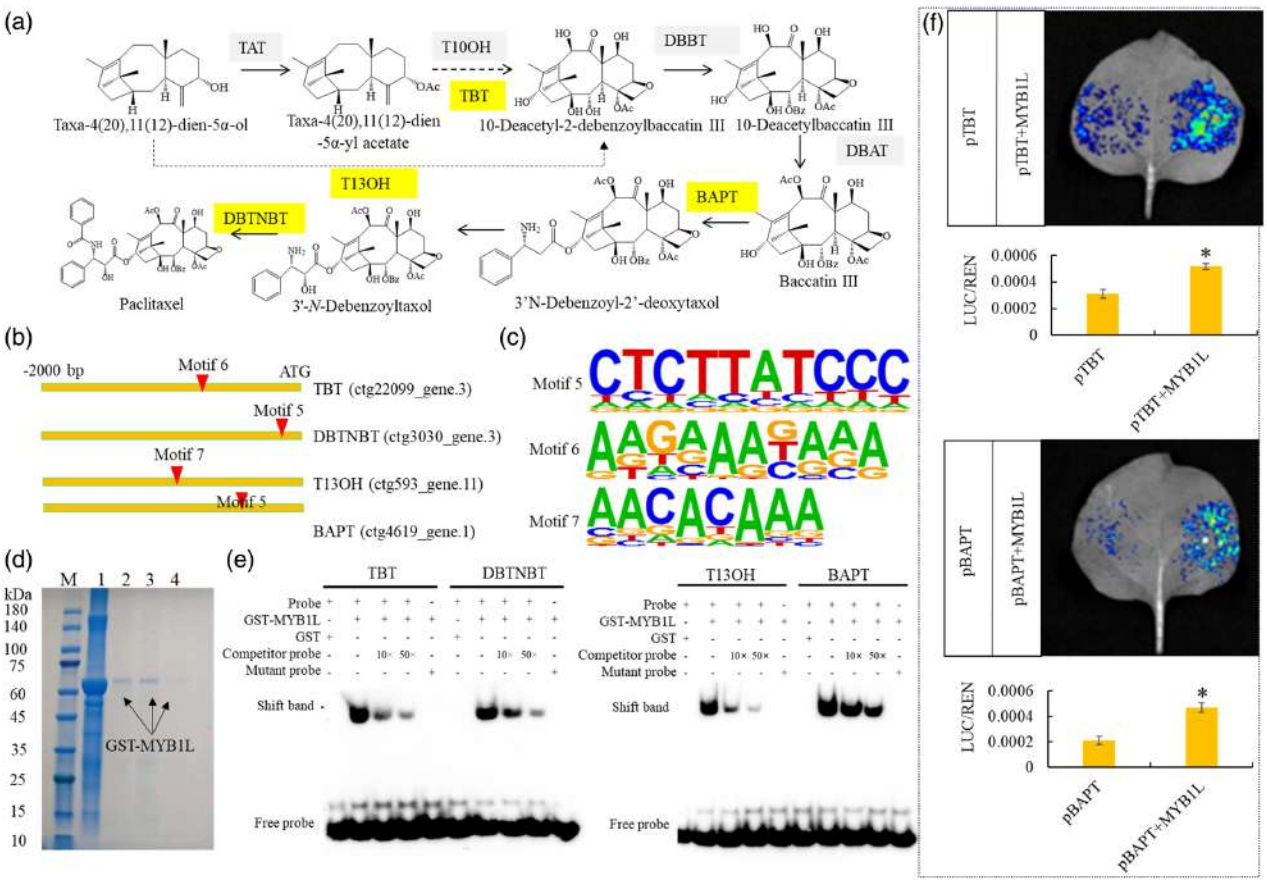

Figure 7. Involvement of MYB1L in the regulation of Taxol biosynthesis.
(a) Overview of the complete Taxol biosynthesis pathway. Yellow backgrounds indicated the targets of MYB1L.
(b) Motif analysis of the four MYB1L target genes.
(c) The sequence logos of the three MYB1L binding motifs.
(d) Expression and affinity purification of the fused GST-MYB1L protein. M, protein marker; lanes 1–4, purification of GST–MYB1L.
(e) Electrophoretic mobility shift assay (EMSA) for the binding of MYB1L to their targets. The GST only or MYB1L-GST fusion protein was incubated with the probes containing the binding elements derived from the promoters. '–'and '+' represent absence and presence, respectively, and '20×' or '200×' show increasing amounts of probes for competition.
(f) The transcriptional abilities analysis of MYB1L using dual-luciferase reporter assay. The detailed value of transcriptional abilities of MYB1L was determined by the LUC/REN ratios. The pBD vector that produced the GAL4 DNA-BD alone was treated as negative control. Three biological repeats were used in the present study. "*" indicated significant changes at $P < 0.05$.

(P = 1e-1578), "CTYTCTYTCTCTCTC" (P = 1e-1265), "TTAACCATAG" (P = 1e-654), and "CKTCKTCTTY" (P = 1e-545) (Table S6). In addition, several *de novo* motifs were found including "GTTTAGGGTTTA" (P = 1e-5182), "GGTATAGG" (P = 1e-2192), "GAGCCATAAG" (P = 1e-1752), "AAGAAGAARAAA" (P = 1e-1669), and "CTCTTATCCC" (P = 1e-1197) (Table S7). Our data have provided new information about MYB recognition sites.

Taxol biosynthesis-related target genes of MYB1L

After searching the target peak pool, four Taxol biosynthesis-related target promoters were identified, including the promoters of the *TBT*, *DBTNBT*, *T13OH*, and *BAPT* genes (Figure 7a). The DAP-seq peaks near the *TBT*, *DBTNBT*, *T13OH*, and *BAPT* genes were visualized using IGV software (Figure S5). Motif analysis showed that MYB1L recognized motif 5 in the *DBTNBT* and *BAPT* promoters, motif 6 in the *TBT* promoter, and motif 7 in the *T13OH* promoter (Figure 7b). The sequence logos of the three MYB1L binding motifs are shown in Figure 7c.

To verify the binding of MYB1L to its potential targets, we successfully overexpressed and affinity-purified the *GST-MYB1L* fusion gene (Figure 7d). Our electrophoretic mobility shift assay (EMSA) data showed that MYB1L directly bound to the motif sequences in the promoters of *TBT*, *DBTNBT*, *T13OH*, and *BAPT* (Figure 7e). Subsequently, we employed a dual-LUC reporter assay to assess the transcriptional activity of MYB1L. We found that MYB1L significantly increased the expression of the *TBT* and *BAPT* genes (Figure 7f). However, no significant effect

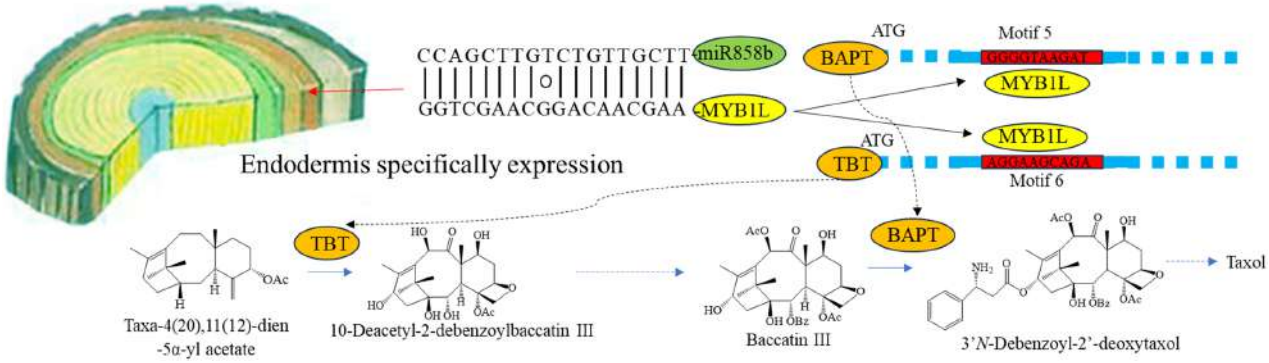

Figure 8. A model for the regulatory roles of MYB1L in Taxol biosynthesis.
MYB1L play important regulatory roles in Taxol biosynthesis by activating the expression of *TBT* and *BAPT* genes.

of MYB1L on the expression of the *DBTNBT* and *T13OH* genes was observed (Figure S6). Collectively, our findings predict a model for the regulatory roles of MYB1L in Taxol biosynthesis and indicate that *TBT* and *BAPT* are downstream target genes of MYB1L (Figure 8).

DISCUSSION

Despite ongoing research on the synthetic biology of Taxol, natural yew resources remain the primary raw material for Taxol extraction (Kou et al., 2024). The accumulation of taxoids varies significantly among different species, environments, and plant tissues (Nasiri et al., 2016). Our findings provide detailed insights into the distribution of taxoids in *T. mairei* stems and may enhance the utilization of *Taxus* trees.

Due to its high content of Taxol, the *Taxus* stem is currently one of the most important raw materials for the industrial extraction of Taxol. Modern chemical analysis techniques have indicated that the distribution of taxoids varies greatly among different stem tissues (Ge et al., 2010). For example, in *T. media*, a high concentration of BAC was found in the wood, while Taxol was shown to accumulate in the phloem and outer bark (Soliman & Raizada, 2020). In *T. mairei*, Taxol enrichment occurred in the phloem, whereas BAC accumulated in the pith (Yu et al., 2020). In the current study, we found that two important intermediates (10-DAB III and BAC) for Taxol biosynthesis were significantly enriched in the pith, while the end product (Taxol) was significantly enriched in the phloem (Figure 2b,c). Furthermore, two Taxol analogues (10-deacetyl-7-xylosylpaclitaxel and 10-deacetylTaxol C) were found to display a similar distribution pattern with Taxol. Our data indicate that intermediates may be transported among different stem tissues.

The accumulation of taxoids has also been shown to be affected by stem age (Mukherjee et al., 2002). In *T. baccata*, a significant difference in the Taxol content of bark from trees of different ages was observed (Nadeem et al., 2002). For example, the tissue culture from young trees contains more C14-OH taxoids and Yunnanxane than that from old trees (Demidova et al., 2023). Furthermore, a decrease in taxoid levels was associated with increasing tree age in the twigs and needles from *T. mairei*, suggesting the important role of young twigs in the extraction of Taxol (Li et al., 2021). In our study, significantly higher levels of taxoids, including 10-DAB III, BAC, Taxol, 10-deacetylTaxol C, and cephalomannine, were found to accumulate in young stems, consistent with previous reports. Our data indicate that newly sprouted branches are the best source of raw material for extracting Taxol. However, current knowledge regarding the effects of stem tissue and age on the accumulation of Taxol remains limited.

Recent advances in MS-based proteomic analysis have significantly enhanced the study of plant tissue samples, thereby promoting the understanding of the regulation of secondary metabolism (Yan et al., 2022). Investigating the spatial distribution of enzymes across different tissues is essential for an in-depth study of secondary metabolism regulation (Blackburn et al., 2022). However, separating plant tissues is a very challenging task in spatial proteomics analysis. To improve accuracy, LCM-DDA-MS/MS was used to analyze the spatial localization information of the target proteins involved in the Taxol biosynthetic pathway. Recent applications of LCM-DDA-MS/MS in plant proteomes have identified 6575 quantifiable proteins in tomato root tips, 3879 quantifiable proteins in cherry tomatoes, and 210–800 peptides in maize kernels (Chen, Huang, et al., 2020; Potts et al., 2022; Yang et al., 2020). Here, LCM-DDA-MS/MS analysis identified 3145 proteins in various *T. mairei* stem tissues, establishing a foundation for a comprehensive analysis of the metabolic pathways. Although the number of proteins identified in different sample groups was relatively uniform, almost no protein was detected in the pith of T stems, indicating that the pith of T stems has become hollow. The MEP pathway supplies the most critical precursor, diterpenoid

taxane core, for the Taxol biosynthetic pathway (Eisenreich et al., 1996). Fortunately, most MEP pathway-related proteins were detected in both O and T stems, suggesting an adequate supply of precursors for Taxol biosynthesis (He et al., 2024). Moreover, several key enzymes, such as T5OH, TAT, T2OH, and BAPT, were highly produced in the O stems, which is the molecular basis for the accumulation of taxoids in young twigs. Interestingly, most of the detected Taxol biosynthesis-related enzymes were produced in the endodermis, especially in the endodermis cells of O stems (O4). Our proteomic data provide a genetic basis for the endodermis-specific accumulation of Taxol, especially in the young stems.

MYB-like proteins belong to a family of highly conserved TFs in plants, animals, and fungi, which participate in the transcriptional regulation of various downstream genes (Feng et al., 2023; Son et al., 2024). Many MYBs have been shown to be involved in the regulation of the Taxol biosynthetic pathway (Cao et al., 2022; Yu et al., 2020; Yu et al., 2022). In 2020, an endodermis-specific MYB, which regulates Taxol biosynthesis by enhancing the expression of *TBT* and *TS* genes, was identified in *T. media* (Yu et al., 2020). In the present study, another endodermis-specific MYB member (MYB1L) was identified by single-cell sequencing. Our *in situ* hybridization experiment confirmed that MYB1L was significantly expressed in the endodermis of young stems, suggesting MYB1L is an important regulator of the endodermis-specific accumulation of Taxol in young twigs.

Recently, a regulatory network mediated by miRNAs in Taxol biosynthesis has been proposed. For example, miR159b-MYB (gK_002135) and miR187-MYB (gK_002135) were reported to be involved in Taxol biosynthesis by targeting *TBT-2*, *TBT-4*, and *GGPPS-1* (Sun et al., 2024). In *T. chinensis*, miR5298b regulates Taxol biosynthesis by activating the NPR3-TGA6 complex, which up-regulates the expression of *DBAT*, *TS*, and *T5OH* genes (Ying et al., 2023). Furthermore, miR858 is an important component of a regulatory module that participates in the transcriptional regulation by mediating the degradation of R2R3-MYB TFs (Wang et al., 2024). Based on the miRNA-MYB regulatory network in *T. mairei*, *MYB1L* was identified as a direct target of *miR858b*. The interaction between miR858b and MYB1L was experimentally validated using 5′ RNA ligase-mediated RACE. Through genetic engineering techniques, researchers can edit the binding sites on *MYB1L*, resulting in the loss of *miR858*'s ability to cleave *MYB1L*. Conversely, transient transformation of *miR858b* may inhibit the Taxol biosynthesis by repressing the expression of *MYB1L*. Our data propose a novel function for the miR858-MYB module in regulating the biosynthesis of Taxol in *Taxus* species. In plants, different miR858-MYB networks regulate the anthocyanin and phenylpropanoid biosynthetic pathways (Li et al., 2019; Li et al., 2020; Sharma et al., 2016). In *Ammopiptanthus nanus*, miR858-MYB87 module mediates the accumulation of anthocyanin under osmotic stress (Sumbur et al., 2023). Transient overexpression of miR858 changed the flavonol metabolism in potato (Lin et al., 2021). Our data propose a novel function for the miR858-MYB module in regulating secondary metabolic pathways in plants.

Previous studies have identified several Taxol biosynthesis-related genes as targets of the MYB family. MYB29a has been shown to regulate expression of the *TS*, *T5OH*, and *DBTNBT* genes in *T. chinensis* (Cao et al., 2022), while in *T. media*, MYB39, together with bHLH13, transactivates *GGPPS* and *T10OH* gene expression (Yu et al., 2022). DAP-seq was performed to screen for unknown targets of MYB1L using MYB1L as the bait protein. Several known MYB-binding motifs, including "AGGGTTTAGGGTTTA," "TAAACCCT," "VYTAGGGCAN," and "NNWWAMCCTAAHWNN," were identified, suggesting that our data were reliable (O'Malley et al., 2016). In *T. chinensis*, MYB29a regulates the expression of *DBTNBT* and *BAPT* by binding to several classic elements, such as CTGTTG, CGGTTG, CCGTTG, TAACAG, CAGTTG, TAACTG, and CGGTTG (Cao et al., 2022). Our data showed that MYB1L regulated the expression of *DBTNBT* and *BAPT* by targeting a common element (CTCTTATCCC), which showed a high similarity to the classic "CTGTTG" and "TAACAG" elements. It is worth mentioning that many *de novo* motifs were also predicted, identifying novel binding sites of MYB1L. Our findings further highlight the diversity of MYB-binding sites, in addition to a few well-established MYB-binding elements, such as (T/C)AAC(G/T)G(A/C/T)(A/C/T), (C/T)NGTT(A/G), ACC(A/T)A(A/C)(T/C), and ACC(A/T)(A/C/T)(A/C/T).

TBT catalyze the conversion of 10-deacetyl-2-debenzoylbaccatin III to 3′-*N*-debenzoyl-2′-deoxytaxol, and thus appear to function in the late-stage reaction steps of the Taxol biosynthetic pathway (Walker & Croteau, 2000). Previous studies have reported several MYB-mediated regulation modules involved in Taxol biosynthesis, such as TmMYB3-TBT and TmMYB39-TBT (Yu et al., 2020; Yu et al., 2022). In *T. mairei*, MYB1L regulates the expression of *TBT* by binding to the *de novo* motif 5, suggesting an important role for MYB1L in taxol biosynthesis. Due to the limited sensitivity of LCM-DDA-MS/MS analysis, the TBT protein was not detected. Therefore, in future studies, the sensitivity of LCM-DDA-MS/MS needs to be improved in order to detect more proteins. Our findings suggest that an integrated analysis of multiple omics techniques may help to uncover interesting biological phenomena.

In summary, MS imaging analysis confirmed the tissue-specific accumulation of Taxol in *T. mairei* stems, especially in young stems. LCM-DDA-MS/MS identified several tissue-specific proteins across five tissue locations,

indicating that Taxol biosynthesis-related enzymes are predominantly localized in the endodermis of young stems. Moreover, the endodermis-specific expression of *MYB1L* and its regulator, *miR858b*, were identified, suggesting a potential function of the miR858b-MYB1L module in regulating secondary metabolism. DAP-seq analysis identified many potential targets of MYB1L, including four Taxol biosynthesis-related genes (*TBT*, *DBTNBT*, *T13OH*, and *BAPT*). Our data revealed that the miR858b-MYB1L axis plays a significant role in the transcriptional regulation of Taxol biosynthesis by enhancing the expression of the *TBT* and *BAPT* genes in the endodermis.

MATERIAL AND METHODS

Plant material and datasets

Seven-year-old *T. mairei* plants were grown in an experimental field at the campus of Hangzhou Normal University, Hangzhou, China. 1-year-old (O) and 2-year-old (T) twigs were collected for MS imaging and LCM experiments. Tissue-specific gene expression was analyzed using a previously published single-cell transcriptome dataset (PRJNA909435). Three independent biological replicates were used for MS imaging and LCM-MS/MS analysis. Chemical structures were drawn using ChemDraw software (ver. 19.0).

Sample preparation and MS imaging

Stem samples were fixed, then cryosectioned to 20 μm slides using a pre-cooled freezing microtome (Leica CM1950). The slides were placed onto a MALDI-2 conductive glass slide and transferred to a vacuum dryer for 30 min for vacuum sealing. MALDI-2 matrix (Bruker, Bremen, Germany) was gently sprayed onto the stem sections using a TM-Sprayer. The substrate-coated slides were then positioned on a target disk on the TimsTOF FLeX MALDI-2 platform (Bruker). The sample site was marked using Bruker data imaging software. Following laser irradiation, the chemical molecules were ionized and released from the target sites on the stem section. The ionized molecules were captured and detected by MS to generate imaging files.

Analysis of MS imaging files

Raw MS imaging files were uploaded into the SCiLS-Lab software (ver. 2021) for data analysis, including baseline correction, peak identification, data smoothing, and data normalization. Imaging sites within the target area were clustered using a non-supervised spatial clustering program. Imaging data points exhibiting similar metabolite accumulation patterns are shown in the same color. Resulting features were compared with the theoretical molecular mass within a 10 ppm mass error in the Bruker MetaboBASE Library metabobase (version 3.0) to identify metabolites. Principal component analysis (PCA) was performed to analyze the distribution of metabolites on the slices.

Slide preparation and LCM

O and T stems were prepared as formalin-fixed paraffin-embedded tissue sections. Slides were dewaxed with xylene, rehydrated in a series of alcohol solutions, stained with hematoxylin & eosin, and visualized using the Leica LCM System (Leica LMD7). For each stem tissue, three independent samples were obtained.

Protein extraction and data-dependent acquisition (DDA) sampling

Protein was extracted from frozen stem samples using TCA/acetone buffer, then added to SDT buffer (4% SDS and 100 mM Tris–HCl, pH 7.6), sonicated, and boiled for 10 min. Samples were then centrifuged at 14000*g* for 30 min. The protein concentration in the supernatants was determined using a Protein Assay Kit (Bio-Rad, USA). The digested peptide solution was fractionated into several fractions using the Thermo Scientific™ Pierce™ High pH Reversed-Phase Peptide Fractionation Kit. Each fraction was desalted using C18 Cartridges (Empore™ SPE Cartridges C18, bed I.D. 7 mm, volume 3 mL, Sigma) and reconstituted in 40 μL 0.1% (v/v) formic acid solution.

DDA-MS/MS analysis

All fractions used for the construction of the DDA library were uploaded to a Thermo Scientific Q-Exactive HF-X-MS with an Easy-nLC 1200 chromatography platform (Thermo Scientific). The peptide solution was separated using an ES802 C18 analytical HPLC column (Thermo Scientific) with a concentration gradient of buffer B containing 84% acetonitrile and 0.1% formic acid. MS features were detected in the positive ion mode, with a scan range of 350–1800 *m/z* and an MS1 scan resolution of 60 000 (200 *m/z*). The automatic gain control (AGC) target was 1E6 with a maximum injection time (IT) of 50 ms and dynamic exclusion of 10 s. The isolation window was set to 1.5 *m/z*, the MS2 scan resolution was set to 30 000 with a maximum IT of 50 ms and normalized collision energy of 30 eV.

Bioinformatic analysis of the DDA library data

For DDA library data analysis, the FASTA sequence database was searched using Biognosys Spectronaut™ software (https://www.uniprot.org). For peptide identification, the maximum missed cleavage allowed was set at 1, fixed modification was set at carbamidomethyl, and dynamic modification was set at oxidation and acetylation. For protein identification, the resulting data were based on 99% confidence as determined by a false discovery rate (FDR) analysis of ≤1%.

Screening and *in situ* hybridization of tissue-specific expressed members of the MYB family of TFs

The same stem samples were harvested and fixed in formalin-aceto-alcohol solution at 4°C. Samples were decolorized by incubating in tert-butyl alcohol in 95% alcohol, then placed in an embedding box and covered in dissolved wax. Wax-embedded samples were sliced into 7 μm-thick sections using a slicer at 4°C. Slides were dried, placed in xylene to remove the wax, then immersed in a series of alcohol solutions with various concentrations. Finally, slides were incubated with 1 μg/mL Proteinase K at room temperature for 20 min to remove potentially contaminating proteins.

In situ hybridization was carried out using a DIG RNA Labeling Kit (SP6/T7). Briefly, slides were incubated with DIG Easy Hyb buffer for 20 min, followed by incubation with DIG Easy Hyb buffer containing a gene probe (10 pg/mL) for 12 h at 42°C. Slices were washed twice with 2 × SSC buffer at 25°C and twice for 20 min at 65°C. Slides were then washed with washing buffer for 5 min, incubated in a closed solution for 2 h, and incubated with an antibody for 2 h at 37°C. After washing, slides were incubated with detection buffer for 5 min, followed by incubation in a substrate chromogenic solution for signal detection.

Small RNA (sRNA) library construction and sequencing

Total RNA was isolated from *T. mairei* stems using TRIzol reagent (Invitrogen, Shanghai, China). Approximately 1 μg RNA was used to construct the sRNA library. sRNAs were generated, then ligated to a sequencing adapter. Following reverse transcription and PCR amplification, a cDNA library was generated for miRNA sequencing. Sequencing was carried out using an Illumina HiSeq 2500 platform (San Diego, USA). Three independent sample groups were used.

Analysis of sRNAs

Raw reads were processed to remove adapter dimers and low-quality sequences using ACGT101-miR (ver. 4.2) software. Then, unique reads were mapped to predicted precursors in miRBase (ver. 22.1) by searching known and unknown miRNAs. During sequence alignment, length variation at both the 3′ and 5′ ends and one mismatch were allowed. Unmapped sequences were read against the *T. mairei* genome, and hairpin structures containing sequences were predicted using RNAfold software (http://rna.tbi.univie.ac.at/).

The target genes of the most abundant miRNAs were predicted using computational algorithms for target prediction (GSTAr, ver. 1.0) that detected miRNA binding sites. Functional analysis of the target genes of miRNAs was carried out using GO and KEGG bioinformatic tools. GO and KEGG enrichment analyses were performed using Fisher's exact test with a P value <0.05.

Preparation of *Taxus* protoplasts

Approximately 500 mg young stems of *Taxus* were harvested, then incubated with 10 mL enzymatic hydrolysate for 3 h at 25°C and centrifuged for 3 min. After discarding the supernatant, the remaining sample was incubated with 10 mL washing solution for 30 min on ice. The supernatant was removed, and the remaining sample was incubated with MMG solution, containing 4 mL 0.4 M mannitol, 2300 mL 15 mM $MgCl_2$, and 400 mL 4 mM MES, up to a concentration of 2×10^5 protoplasts/mL. Next, 200 μL protoplast suspension, 20 μL vector plasmid, and 220 μL PEG solution were mixed and incubated at 25°C for 15 min. The reaction was terminated by adding 1 mL washing solution.

Dual-luciferase (dual-LUC) reporter assay

Cell lysis was carried out by incubating protoplasts in 100 μL cell lysis buffer for 5 min at 25°C. Following centrifugation at 12500 g for 10 min, supernatants were collected for subsequent analysis. Next, 100 μL firefly luciferase substrate was added to the supernatants in ELISA plates, and the activity of the firefly luciferase reporter gene was immediately detected using a fluorescence detector. After, 100 μL freshly prepared *Renilla* substrate working buffer was added to the reaction solution, and the activity of the *Renilla* luciferase reporter gene was quickly detected with a fluorescence detector. Each test was performed in triplicate.

Prokaryotic expression vectors and western blotting analysis

The full-length encoding sequence of the *MYB1L* gene was inserted into the pET30a vector. The recombinant MYB1L protein with a Halo-tag was expressed by *Escherichia coli* cells. Recombinant proteins were purified using beads with a Halo-tag antibody. Expression of the MYB1L-Halo protein was determined by western blotting analysis. Approximately 10 μg protein from different tissues was separated by 12% SDS-PAGE and transferred to a polyvinyl difluoride membrane. Membranes were incubated with a polyclonal antibody against Halo-MYB1L (1:100). The MYB1L protein band was visualized using the ECL Western Blot Detection and Analysis System (GE Healthcare) according to the manufacturer's protocol.

Construction of the DNA library and DNA-binding assays

Genomic DNA was extracted from *T. mairei* stems, fragmented, and ligated to a sequencing adapter to construct a DAP-seq library. The MYB1L protein with a Halo affinity tag was produced by prokaryotic expression and purified using G7281Magne Halo-tag beads (Promega). Genomic DNA was incubated with the affinity-bound MYB1L protein. The *T. mairei* MYB1L-Halo-tag fusion protein and 500 ng genomic library DNAs were incubated in 100 μL PBS buffer with gentle shaking for 2 h at 4°C. Unbound DNA was removed by washing five times with washing buffer (200 μL PBS + 0.005% NP40). MYB1L-bound miRNAs were eluted and amplified by PCR to produce an indexed adapter and sequence. The mock DAP-seq libraries were treated as negative controls.

DAP-seq data analysis

DAP-seq was performed on the Illumina NovaSeq 6000 system using the PE150 method. The experiment was repeated twice (MYB-1 and MYB-2). Clean reads were mapped to the reference genome sequence using BWA software with the MEM method. The length of the inserted segment was calculated based on the comparison between the two ends of the reads. The Model-Based Analysis of ChIP-Seq algorithm (ver. 2.2.7.1) was used to identify binding peaks. Genes containing binding peaks located within 3 kb upstream of the transcription start site (TSS) or downstream of the transcription termination site (TTS) were defined as targets of MYB1L. Motif analysis of the peak region was performed using the HOMER (Hypergeometric Optimization of Motif Enrichment) program. Representative DAPseq peaks were visualized using Integrative Genomics Viewer software (ver. 2.16.0).

Electrophoretic mobility shift assay (EMSA) and dual-LUC reporter assay experiments for TF-target validation

The full-length sequence of MYB1L was inserted into the pET30a vector and expressed in *E. coli* to produce recombinant His-MYB1L protein. Proteins were purified using Clontech His60 Ni Superflow Resin. EMSA was carried out using the GS009 Light Shift Chemiluminescent EMSA Kit (Beyotime, China) as described in our previous study (Zhan et al., 2023).

The 1500 bp promoter regions of four Taxol biosynthesis-related genes, including *TBT* (ctg22099_gene.3), *DBTNBT* (ctg3030_gene.3), *T13OH* (ctg593_gene.11), and *BAPT* (ctg4619_gene.1), were extracted and cloned into the pGreenII0800-LUC vector to construct reporters. The full-length sequence of *MYB1L* was inserted into the pGreenII62-SK vector to generate an effector plasmid. GAL4-BD and VP-16 were treated as positive and negative controls, respectively. The resulting constructs were transfected into the stems of *Taxus* by GV3101-mediated transient expression. Firefly luciferase (LUC) and *Renilla* luciferase (REN) activities were analyzed using a Dual-Luciferase Reporter Assay Kit (Promega, Madison, USA).

AUTHOR CONTRIBUTIONS

CY and CS conceptualized the initial study; CY, DZ, XZ, YZ, and ZF were involved in the experimental layout; CY, DZ,

XZ, ZF, WL, MZ, EB, and YZ performed the lab experiments; CY and CS drafted the initial article; all authors discussed the results, reviewed the article, and approved the final article.

ACKNOWLEDGMENTS

This work was funded by the National Natural Science Foundation of China (32270382 and 32271905); the Zhejiang Provincial Natural Science Foundation of China under Grant (No. LY23C160001). We are grateful to LC Sciences company (Hangzhou, China) and Shanghai Applied Protein Technology Co., Ltd (Shanghai, China) for transcriptomic and metabolomic analysis, respectively.

CONFLICT OF INTEREST

The authors have no relevant financial or non-financial interests to disclose.

DATA AVAILABILITY STATEMENT

The data that supports the findings of this study are available in the supplementary material of this article.

SUPPORTING INFORMATION

Additional Supporting Information may be found in the online version of this article.

Figure S1. Overview of the MS imaging data. (a) MALDI-IMS was performed to examine the tissue-specific accumulation of taxoids. (b) segmentation analysis of the samples from two groups. (c) The number of data points in each sample. (d) K means-based maps revealed the presence of several tissue-specific metabolite accumulation patterns in samples.

Figure S2. Overview of the DDA-MS/MS data. Analysis of two quality control parameters, protein FDR (a) and protein abundance (b). (c) 3D PCA of all the samples.

Figure S3. Multiple sequence alignment analysis of MYB1L. Red box indicated the R2 and R3 domains.

Figure S4. Functional annotation of the putative miRNA targets. (a) GO enrichment analysis grouped all of the predicted targets into four categories. (b) KEGG enrichment analysis suggested that the predicted targets might be involved in various metabolic pathways.

Figure S5. Visualization of the DAP-seq peaks near the TBT, DBTNBT, T13OH, and BAPT genes. MYB1 and MYB2 are two biological repeats. MYB_input is control.

Figure S6. The transcription analysis of MYB1L using dual-luciferase reporter assay. (a) The detailed value of transcriptional abilities of MYB1L on DBTNBT was determined by the LUC/REN ratios. (b) The detailed value of transcriptional abilities of MYB1L on T13OH was determined by the LUC/REN ratios. The pBD vector that produced the GAL4 DNA-BD alone was treated as negative control. Three biological repeats were used in the present study

Table S1. The detailed information of the detected MS features.

Table S2. The detailed information of the proteins from LCM-DDA-MS/MS analysis.

Table S3. The detailed information of the miRNA target genes.

Table S4. The detailed information of the sequencing reads from three libraries.

Table S5. The detailed information of the MYB1L target peaks.

Table S6. Motif enrichment analysis of the known MYB1L binding motifs.

Table S7. Motif enrichment analysis of the de novo MYB1L binding motifs.

REFERENCES

Arendowski, A. & **Ruman, T.** (2017) Laser desorption/ionisation mass spectrometry imaging of European yew (*Taxus baccata*) on gold nanoparticle-enhanced target. *Phytochemical Analysis*, **28**, 448–453.

Blackburn, M.R., **Minkoff, B.B.** & **Sussman, M.R.** (2022) Mass spectrometry-based technologies for probing the 3D world of plant proteins. *Plant Physiology*, **189**, 12–22.

Bobadilla, L.K. & **Tranel, P.J.** (2024) Predicting the unpredictable: the regulatory nature and promiscuity of herbicide cross resistance. *Pest Management Science*, **80**, 235–244.

Cao, X., **Xu, L.**, **Li, L.**, **Wan, W.** & **Jiang, J.** (2022) TcMYB29a, an ABA-responsive R2R3-MYB transcriptional factor, upregulates Taxol biosynthesis in *Taxus chinensis*. *Frontiers in Plant Science*, **13**, 804593.

Cao, Y., **Li, K.**, **Li, Y.**, **Zhao, X.** & **Wang, L.** (2020) MYB transcription factors as regulators of secondary metabolism in plants. *Biology (Basel)*, **9**, 61.

Chen, Q., **Huang, R.**, **Xu, Z.**, **Zhang, Y.**, **Li, L.**, **Fu, J.** ***et al.*** (2020) Label-free comparative proteomic analysis combined with laser-capture microdissection suggests important roles of stress responses in the black layer of maize kernels. *International Journal of Molecular Sciences*, **21**, 1369.

Chen, Y., **Zhang, H.**, **Zhang, M.**, **Zhang, W.**, **Ou, Z.**, **Peng, Z.** ***et al.*** (2021) Salicylic acid-responsive factor TcWRKY33 positively regulates Taxol biosynthesis in *Taxus chinensis* in direct and indirect ways. *Frontiers in Plant Science*, **12**, 697476.

Chen, Y., **Zhang, M.**, **Jin, X.**, **Tao, H.**, **Wang, Y.**, **Peng, B.** ***et al.*** (2020) Transcriptional reprogramming strategies and miRNA-mediated regulation networks of Taxus media induced into callus cells from tissues. *BMC Genomics*, **21**, 168.

Chybicki, I.J. & **Oleksa, A.** (2018) Seed and pollen gene dispersal in Taxus baccata, a dioecious conifer in the face of strong population fragmentation. *Annals of Botany*, **122**, 409–421.

Das, T., **Kumar Pandey, D.**, **Shekhawat, M.S.**, **Dey, A.** & **Malik, T.** (2023) Quantification of tissue-specific paclitaxel in Himalayan yew using HPTLC-Densitometric analysis, assessment of toxicological activity, and tissue-specific evaluation of antioxidant activity. *ACS Omega*, **8**, 32108–32118.

Demidova, E., **Globa, E.**, **Klushin, A.**, **Kochkin, D.** & **Nosov, A.** (2023) Effect of methyl Jasmonate on the growth and biosynthesis of C13- and C14-Hydroxylated Taxoids in the cell culture of yew (*Taxus wallichiana* Zucc.) of different ages. *Biomolecules*, **13**, 969.

Eisenreich, W., **Menhard, B.**, **Hylands, P.J.**, **Zenk, M.H.** & **Bacher, A.** (1996) Studies on the biosynthesis of taxol: the taxane carbon skeleton is not of mevalonoid origin. *Proceedings of the National Academy of Sciences of the United States of America*, **93**, 6431–6436.

Fei, Y., **Luo, C.** & **Tang, W.** (2019) Differential expression of MicroRNAs during root formation in *Taxus Chinensis* Var. mairei cultivars. *Open Life Sciences*, **14**, 97–109.

Feng, S., **Hou, K.**, **Zhang, H.**, **Chen, C.**, **Huang, J.**, **Wu, Q.** ***et al.*** (2023) Investigation of the role of TmMYB16/123 and their targets (TmMTP1/11) in the tolerance of *Taxus media* to cadmium. *Tree Physiology*, **43**, 1009–1022.

Gallego-Jara, J., **Lozano-Terol, G.**, **Sola-Martínez, R.A.**, **Cánovas-Díaz, M.** & **de Diego Puente, T.** (2020) A compressive review about Taxol(®): history and future challenges. *Molecules*, **25**, 5986.

Ge, G.B., **Liang, S.C.**, **Hu, Y.**, **Liu, X.B.**, **Mao, Y.X.**, **Zhang, Y.Y.** ***et al.*** (2010) Rapid qualitative and quantitative determination of seven valuable taxanes from various *Taxus* species by UFLC-ESI-MS and UFLC-DAD. *Planta Medica*, **76**, 1773–1777.

Hao, D.C., **Yang, L.**, **Xiao, P.G.** & **Liu, M.** (2012) Identification of *Taxus* microRNAs and their targets with high-throughput sequencing and degradome analysis. *Physiologia Plantarum*, **146**, 388–403.

He, S., **Bekhof, A.M.W.**, **Popova, E.Z.**, **van Merkerk, R.** & **Quax, W.J.** (2024) Improved taxadiene production by optimizing DXS expression and fusing short-chain prenyltransferases. *New Biotechnology*, **83**, 66–73.

Hobert, O. (2008) Gene regulation by transcription factors and MicroRNAs. *Science*, **319**, 1785–1786.

Jennewein, S., **Wildung, M.R.**, **Chau, M.**, **Walker, K.** & **Croteau, R.** (2004) Random sequencing of an induced Taxus cell cDNA library for identification of clones involved in Taxol biosynthesis. *Proceedings of the National Academy of Sciences of the United States of America*, **101**, 9149–9154.

Jiang, B., **Gao, L.**, **Wang, H.**, **Sun, Y.**, **Zhang, X.**, **Ke, H.** ***et al.*** (2024) Characterization and heterologous reconstitution of Taxus biosynthetic enzymes leading to baccatin III. *Science*, **383**, 622–629.

Kaspera, R. & **Croteau, R.** (2006) Cytochrome P450 oxygenases of Taxol biosynthesis. *Phytochemistry Reviews: Proceedings of the Phytochemical Society of Europe*, **5**, 433–444.

Kou, P., **Yu, Y.**, **Wang, H.**, **Zhang, Y.**, **Jin, Z.** & **Yu, F.** (2024) An integrated strategy based on 10-DAB extraction and in situ whole-cell biotransformation of renewable Taxus needles to produce Baccatin III. *Molecules*, **29**, 2586.

Kuang, X., **Sun, S.**, **Wei, J.**, **Li, Y.** & **Sun, C.** (2019) Iso-Seq analysis of the Taxus cuspidata transcriptome reveals the complexity of Taxol biosynthesis. *BMC Plant Biology*, **19**, 210.

Li, H., **Zhang, S.**, **Zhao, Y.**, **He, J.** & **Chen, X.** (2023) Identification of raffinose family oligosaccharides in processed *Rehmannia glutinosa* Libosch using matrix-assisted laser desorption/ionization mass spectrometry image combined with machine learning. *Rapid Communications in Mass Spectrometry*, **37**, e9635.

Li, L., **Chen, Y.**, **Ma, Y.**, **Wang, Z.**, **Wang, T.** & **Xie, Y.** (2021) Optimization of Taxol extraction process using response surface methodology and investigation of temporal and spatial distribution of Taxol in *Taxus mairei*. *Molecules*, **26**, 5485.

Li, Y., **Cui, W.**, **Qi, X.**, **Lin, M.**, **Qiao, C.**, **Zhong, Y.** ***et al.*** (2020) MicroRNA858 negatively regulates anthocyanin biosynthesis by repressing AaMYBC1 expression in kiwifruit (*Actinidia arguta*). *Plant Science*, **296**, 110476.

Li, Y., **Cui, W.**, **Wang, R.**, **Lin, M.**, **Zhong, Y.**, **Sun, L.** ***et al.*** (2019) MicroRNA858-mediated regulation of anthocyanin biosynthesis in kiwifruit (Actinidia arguta) based on small RNA sequencing. *PLoS One*, **14**, e0217480.

Lin, S., **Singh, R.K.**, **Moehninsi, S.** & **Navarre, D.A.** (2021) R2R3-MYB transcription factors, StmiR858 and sucrose mediate potato flavonol biosynthesis. *Horticulture Research*, **8**, 25.

Mukherjee, S., **Ghosh, B.**, **Jha, T.B.** & **Jha, S.** (2002) Variation in content of taxol and related taxanes in eastern Himalayan populations of Taxus wallichiana. *Planta Medica*, **68**, 757–759.

Nadeem, M., **Rikhari, H.C.**, **Kumar, A.**, **Palni, L.M.** & **Nandi, S.K.** (2002) Taxol content in the bark of Himalayan yew in relation to tree age and sex. *Phytochemistry*, **60**, 627–631.

Nasiri, J., **Naghavi, M.R.**, **Alizadeh, H.** & **Moghadam, M.R.** (2016) Seasonal-based temporal changes fluctuate expression patterns of *TXS*, *DBAT*, *BAPT* and *DBTNBT* genes alongside production of associated taxanes in *Taxus baccata*. *Plant Cell Reports*, **35**, 1103–1119.

O'Malley, R.C., **Huang, S.C.**, **Song, L.**, **Lewsey, M.G.**, **Bartlett, A.**, **Nery, J.R.** ***et al.*** (2016) Cistrome and Epicistrome features shape the regulatory DNA landscape. *Cell*, **165**, 1280–1292.

Potts, J., **Li, H.**, **Qin, Y.**, **Wu, X.**, **Hui, D.**, **Nasr, K.A.** ***et al.*** (2022) Using single cell type proteomics to identify Al-induced proteomes in outer layer cells and interior tissues in the apical meristem/cell division regions of tomato root-tips. *Journal of Proteomics*, **255**, 104486.

Schmitz, R.J., **Grotewold, E.** & **Stam, M.** (2022) *Cis*-regulatory sequences in plants: their importance, discovery, and future challenges. *Plant Cell*, **34**, 718–741.

Sharma, D., **Tiwari, M.**, **Pandey, A.**, **Bhatia, C.**, **Sharma, A.** & **Trivedi, P.K.** (2016) MicroRNA858 is a potential regulator of Phenylpropanoid pathway and plant development. *Plant Physiology*, **171**, 944–959.

Shi, X., **Xu, Z.**, **Fu, S.**, **Zhang, X.**, **He, Z.** & **Du, H.** (2010) Effects of gathering season and three age affect on main active components of *Taxus madia*. *Zhongguo Zhong Yao Za Zhi*, **35**, 2538–2540.

Soliman, S.S.M. & **Raizada, M.N.** (2020) Sites of biosynthesis and storage of Taxol in *Taxus media* (Rehder) plants: mechanism of accumulation. *Phytochemistry*, **175**, 112369.

Son, Y.E., **Cho, H.J.** & **Park, H.S.** (2024) The MYB-like protein MylA contributes to conidiogenesis and conidial germination in *aspergillus nidulans*. *Communications Biology*, **7**, 768.

Sumbur, B., **Gao, F.**, **Liu, Q.**, **Feng, D.**, **Bing, J.**, **Dorjee, T.** ***et al.*** (2023) The characterization of R2R3-MYB genes in *Ammopiptanthus nanus* uncovers that the miR858-AnaMYB87 module mediates the accumulation of anthocyanin under osmotic stress. *Biomolecules*, **13**, 1721.

Sun, M.S., **Jia, Y.**, **Chen, X.Y.**, **Chen, J.S.**, **Guo, Y.**, **Fu, F.F.** ***et al.*** (2024) Regulatory microRNAs and phasiRNAs of paclitaxel biosynthesis in Taxus chinensis. *Frontiers in Plant Science*, **15**, 1403060.

Vance, N.C., **Kelsey, R.G.** & **Sabin, T.E.** (1994) Seasonal and tissue variation in taxane concentrations of *Taxus brevifolia*. *Phytochemistry*, **36**, 1241–1244.

Walker, K. & **Croteau, R.** (2000) Taxol biosynthesis: molecular cloning of a benzoyl-CoA:taxane 2alpha-O-benzoyltransferase cDNA from taxus and functional expression in *Escherichia coli*. *Proceedings of the National Academy of Sciences of the United States of America*, **97**, 13591–13596.

Wang, W.Q., **Liu, X.F.**, **Zhu, Y.J.**, **Zhu, J.Z.**, **Liu, C.**, **Wang, Z.Y.** ***et al.*** (2024) Identification of miRNA858 long-loop precursors in seed plants. *Plant Cell*, **36**, 1637–1654.

Wani, M.C. & **Horwitz, S.B.** (2014) Nature as a remarkable chemist: a personal story of the discovery and development of Taxol. *Anti-Cancer Drugs*, **25**, 482–487.

Wildung, M.R. & **Croteau, R.** (1996) A cDNA clone for taxadiene synthase, the diterpene cyclase that catalyzes the committed step of taxol biosynthesis. *The Journal of Biological Chemistry*, **271**, 9201–9204.

Xiong, X., **Gou, J.**, **Liao, Q.**, **Li, Y.**, **Zhou, Q.**, **Bi, G.** ***et al.*** (2021) The Taxus genome provides insights into paclitaxel biosynthesis. *Nature Plants*, **7**, 1026–1036.

Yan, S., **Bhawal, R.**, **Yin, Z.**, **Thannhauser, T.W.** & **Zhang, S.** (2022) Recent advances in proteomics and metabolomics in plants. *Molecular Horticulture*, **2**, 17.

Yang, S., **Li, H.**, **Bhatti, S.**, **Zhou, S.**, **Yang, Y.**, **Fish, T.** ***et al.*** (2020) The Al-induced proteomes of epidermal and outer cortical cells in root apex of cherry tomato 'LA 2710'. *Journal of Proteomics*, **211**, 103560.

Ying, C., **Meng, Z.**, **Wenli, Z.**, **Yamin, W.**, **Hua, Z.**, **Liu, Y.** ***et al.*** (2023) miR5298b regulated taxol biosynthesis by acting on TcNPR3, resulting in an alleviation of the strong inhibition of the TcNPR3-TcTGA6 complex in Taxus chinensis. *International Journal of Biological Macromolecules*, **248**, 125909.

Yu, C., **Hou, K.**, **Zhang, H.**, **Liang, X.**, **Chen, C.**, **Wang, Z.** ***et al.*** (2023) Integrated mass spectrometry imaging and single-cell transcriptome atlas strategies provide novel insights into taxoid biosynthesis and transport in Taxus mairei stems. *The Plant Journal: For Cell and Molecular Biology*, **115**(5), 1243–1260.

Yu, C., **Huang, J.**, **Wu, Q.**, **Zhang, C.**, **Li, X.L.**, **Xu, X.** ***et al.*** (2022) Role of female-predominant MYB39-bHLH13 complex in sexually dimorphic accumulation of taxol in Taxus media. *Horticulture Research*, **9**, uhac062.

Yu, C., **Luo, X.**, **Zhang, C.**, **Xu, X.**, **Huang, J.**, **Chen, Y.** ***et al.*** (2020) Tissue-specific study across the stem of *Taxus media* identifies a phloem-specific TmMYB3 involved in the transcriptional regulation of paclitaxel biosynthesis. *The Plant Journal: For Cell and Molecular Biology*, **103**, 95–110.

Zhan, X., **Liang, X.**, **Lin, W.**, **Ma, R.**, **Zang, Y.**, **Wang, H.** ***et al.*** (2024) Cell type specific regulation of phenolic acid and flavonoid metabolism in Taxus mairei leaves. *Industrial Crops and Products*, **219**, 118975.

Zhan, X., **Qiu, T.**, **Zhang, H.**, **Hou, K.**, **Liang, X.**, **Chen, C.** ***et al.*** (2023) Mass spectrometry imaging and single-cell transcriptional profiling reveal the tissue-specific regulation of bioactive ingredient biosynthesis in *Taxus* leaves. *Plant Communications*, **4**, 100630.

Zhan, X., **Zang, Y.**, **Ma, R.**, **Lin, W.**, **Li, X.L.**, **Pei, Y.** ***et al.*** (2024) Mass spectrometry-imaging analysis of active ingredients in the leaves of *Taxus cuspidata*. *ACS Omega*, **9**, 18634–18642.

Zhang, H., **Hou, K.**, **Liang, X.**, **Lin, W.**, **Ma, R.**, **Zang, Y.** ***et al.*** (2024) Sex-specific responses of *Taxus mairei* to UV-B radiation involved altering the interactions between the microbiota assembly and host secondary metabolism. *Microbiome*, **12**, 165.

Zhang, M., **Jin, X.**, **Chen, Y.**, **Wei, M.**, **Liao, W.**, **Zhao, S.** ***et al.*** (2018) TcMYC2a, a basic helix-loop-helix transcription factor, transduces JA-signals and regulates Taxol biosynthesis in *Taxus chinensis*. *Frontiers in Plant Science*, **9**, 863.

Zhou, T., **Luo, X.**, **Yu, C.**, **Zhang, C.**, **Zhang, L.**, **Song, Y.B.** ***et al.*** (2019) Transcriptome analyses provide insights into the expression pattern and sequence similarity of several taxol biosynthesis-related genes in three Taxus species. *BMC Plant Biology*, **19**, 33.